An EIS alternative for impedance measurement of a high temperature PEM fuel cell stack based on current pulse injection

Jeppesen, Christian; Araya, Samuel Simon; Sahlin, Simon Lennart; Andreasen, Søren Juhl; Kær, Søren Knudsen

Published in:
International Journal of Hydrogen Energy

DOI (link to publication from Publisher):
10.1016/j.ijhydene.2017.05.066

Publication date:
2017

Document Version
Early version, also known as pre-print

An EIS alternative for Impedance Measurement of a High Temperature PEM Fuel Cell Stack Based on Current Pulse Injection

Christian Jeppesen[a,*], Samuel Simon Araya[a], Simon Lennart Sahlin[a], Søren Juhl Andreasen[b], Søren Knudsen Kær[a,*]

[a]*Department of Energy Technology, Aalborg University, Pontoppidanstræde 111, 9220 Aalborg Ø, Denmark*
[b]*Serenergy A/S, Lyngvej 8, 9000 Aalborg, Denmark*

Abstract

In this paper a method for estimating the fuel cell impedance is presented, namely the current pulse injection (CPI) method, which is well suited for online implementation. This method estimates the fuel cell impedance and unlike electrochemical impedance spectroscopy (EIS), it is simple to implement at a low cost. This makes it appealing as a characterization method for on-line diagnostic algorithms. In this work a parameter estimation method for estimation of equivalent electrical circuit (EEC) parameters, which is suited for on-line use is proposed. Tests on a 10 cell high temperature PEM fuel cell show that the method yields consistent results in estimating EEC parameters for different current pulse at different current loads, with a low variance. A comparison with EIS shows that despite its simplicity the response of CPI can reproduce well the impedance response of the high and intermediate frequencies.

Keywords: Fuel Cell, PEM, characterization, EIS, CPI, Current Pulse Injection

Nomenclature

V_{FC}	fuel cell voltage
$\hat{V}_{FC}$	model estimate of fuel cell voltage
V_{OC}	open circuit voltage
I_{FC}	fuel cell DC current
I_{CPI}	current pulse amplitude
R_S	resistor
R_1	parallel resistance
C_1	parallel capacitance
T_s	sampling time
Z	impedance
$\{a_1,b_1,b_2\}$	model parameters
k	current sample
$\hat{\underline{\theta}}$	model parameter vector estimate
$\underline{\underline{\phi}}$	dataset matrix
J	cost function
ϵ	model error
f_s	sampling frequency
f_{CPI}	frequency of pulses
σ^2	parameter variance
j	complex math operator
φ	signal phase
ω	sinusoidal angular frequency

*Corresponding author
Email addresses: chj@et.aau.dk (Christian Jeppesen), skk@et.aau.dk (Søren Knudsen Kær)
URL: http://et.aau.dk (Christian Jeppesen)

1. Introduction

In recent years, the environmental effect of the rising temperatures around the world, has been gaining attention from politicians. The consequences of climate change are being more widely accepted in the general public, and the approval of renewable energy sources is increasing. With more fluctuating renewable energy sources providing power for the electrical grid, new storage solutions that can balance the grid are necessary [1]. Hydrogen produced from water electrolysis using renewable electricity can be a viable option as an energy carrier, which among other things can be used in fuel cells both for stationary and mobile power generation.

The Department of Energy (DoE) in USA, has set a target for fuel cell price and durability for stationary and transport applications. For fuel cells to be competitive the lifetime of a fuel cell must exceed 5000 hours for transport applications and 40000 for stationary applications [2]. During the last decade the durability of fuel cells has improved significantly, due to extensive research in the field and experiences from the industry. However, the lifetime span is still has not reached the targets yet.

For improving the durability of advanced systems such as fuel cells, it is crucial that a proper online diagnostic system is deployed [3]. Such a system could detect faults early, and through a mitigation strategy change the system settings and prevent rapid degradation of the fuel cell stack. Furthermore, a well-designed diagnostic system, could be a part of a prognostics system, which could predict component failure to manage service of the fuel cell system, thus reducing the down time of the systems.

When dealing with diagnostics of fuel cells, the majority of

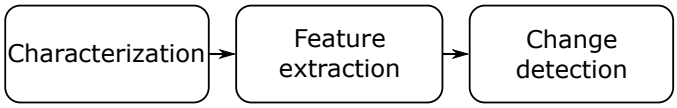

Figure 1: Flow chart of most available model based methods for fuel cell fault detection.

methods available in the literature treats the topic of fault detection in three parts, as shown in Figure 1 [4, 5]. In many studies the fuel cell fault detection is done by detecting a change in the parameters of an equivalent electrical circuit (EEC) model of the fuel cell's dynamic voltage behavior. The most used technique for obtaining EECs model is electrochemical impedance spectroscopy (EIS) [6, 7], with current interruption (CI) method also used to some extent [8, 9]. The former yields the full impedance response and the latter primarily yields a simpler response and often only the ohmic resistance is extracted.

An alternative method for estimating the impedance of an electrochemical device is the Current Pulse Injection (CPI) method. This method is widely used in the battery community, for estimating the state of charge and the state of health [10, 11, 12, 13]. The CPI characterization method works by drawing a small current pulse from the electrochemical device, and then measuring the corresponding transient voltage. By using the current as input and the fuel cell stack voltage as output, an input/output parameter estimation methods can be utilized for estimate the parameters of a EEC model.

In the fuel cell community, different papers have focused on the transient voltage during current steps as a method for fuel cell characterization [14, 15, 16, 17, 18], but not as a diagnostics tool for fuel cells. In [19], small current pulses have been used for estimating EEC model parameters. In another paper, the CPI method was treated in relation to diagnostics of PEM fuel cells, however with a limited access to experimental data and a parameter estimation method not suited for online fuel cell diagnostics [20].

In this work, the CPI method will be used for impedance characterization of a fuel cell short stack, and EEC model parameter estimation method suited for online deployment are suggested. Furthermore, the CPI method performance is compared to the electrochemical impedance spectroscopy characterization method.

2. Methodology

In section presents the current pulse injection method and the implementation. Furthermore, a parameter estimation algorithm for estimation of EEC model parameters is presented. In the end of the section, the experimental setup will be explained.

2.1. Current Pulse Injection method

Current Pulse Injection (CPI) method is an alternative fuel cell characterization method that utilizes small current pulses in the form of an extra drawn current step in a small period of time. Based on the corresponding transient voltage time signals, the

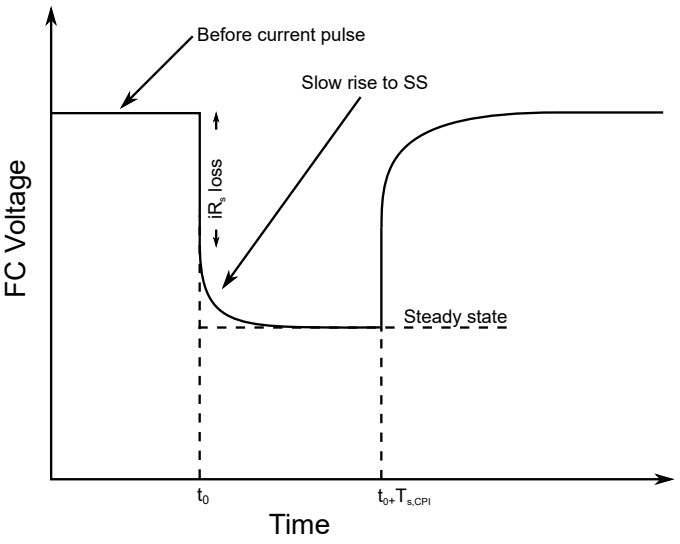

Figure 2: Conceptual drawing of transient voltage durring a small current step.

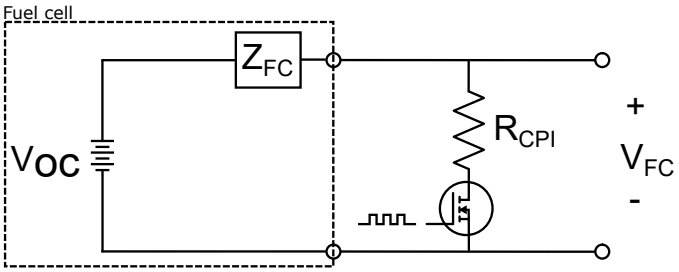

Figure 3: Electrical implementation of the current pulse injection characterization method.

fuel cell impedance can be estimated, by standard available system identification methods. A conceptual voltage profile of a fuel cell voltage is shown in Figure 2, during a small current step. The EEC model estimated based on the CPI method is in general simpler than what can be observed by EIS measurements, but for some diagnostic purposes this technique could be proven sufficient.

The EIS and CPI characterization methods can be conducted in-situ contrary to the CI method, as for the CI method the load must completely be discontinued.

The EIS method is very expensive on lab scale, and even though there are European projects, such as the D-code project (FCH JU, grant No 256673), working on implementing the EIS measurement on an onboard DC-DC converter for fuel cell systems, it still has strict requirements to the bandwidth of the DC-DC converter. The idea behind EIS measurements is simple but will still require a great deal of engineering before it can run on real life fuel cell systems.

The main advantage of the CPI method is that it can be implemented at relatively low cost. As shown in Figure 3, the current pulses used for the CPI method can be implemented by a series resistor and transistor in parallel with the fuel cell terminals. By controlling the transistor with a PWM signal the small electrical circuit will then draw small current pulses from the fuel cell, depending on the size of the resistor.

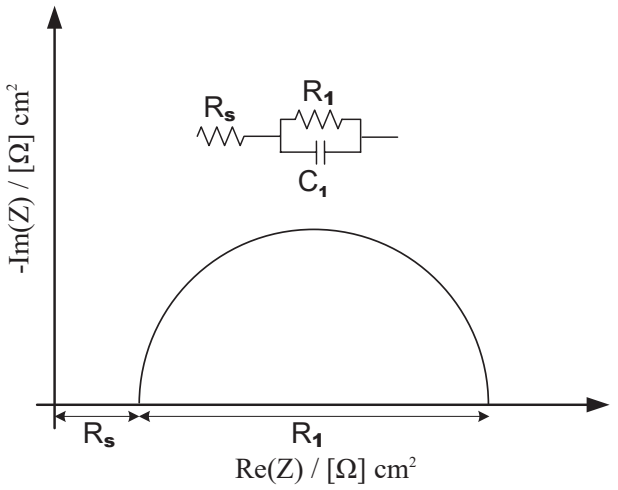

Figure 4: Conceptual Nyquist plot of the EEC model used for the CPI method.

In order to use CPI method for estimating the impedance of a fuel cell, a common approach is to use a parameter estimation method to fit the voltage response to an EEC model. Most fuel cell EEC models utilize a form of the Randles circuit, with 1-3 parallel RC loops. For this work a Randles circuit with one parallel RC loop is used, giving one semicircle in the complex plane, as shown in Figure 4. This is a quite simple circuit, giving a simple response, and yielding a similar transient response as shown in Figure 2. The advantage of such a simple model is that it has lower fitting times and a more consistent parameter fitting algorithm performance and parameter space. Furthermore, as reported in [21], a more complex model might yield a better fit to the data, but at the same time becomes more sensitive to small variations such as measurement noise, and it is therefore the recommendation by Vang et al. [21] to use the less complex EEC models if their accuracy is sufficient for the application.

2.1.1. Parameter estimation algorithm

There are many different methods available for parameter estimation of fuel cell systems, such as EEC models. An extensive review and collection of these methods are available in Ljung's work on system identification [22].

The most common methods available utilize a model prediction error (ϵ), which is the difference between the measured value and the output of a model. The parameter estimation method then aims to minimize the prediction error, and is thereby treated as an optimization problem. For this work a non-recursive least squares method is applied for estimating the parameters of the EEC model, shown in Figure 4. The optimization problem is solved as a linear regression problem, where the prediction error is defined as shown in equation 1, where $\underline{V}_{FC}$ is a column vector of the measured voltage of N length of dataset used for the parameter estimation, and $\underline{\hat{V}}_{FC}$ is a column vector of the model output also of length N.

$$\underline{\epsilon} = \underline{V}_{FC} - \underline{\hat{V}}_{FC} \tag{1}$$

The model output $\hat{V}_{FC}$, which is a mathematical representation of V_{FC}, can be described as the open circuit voltage (V_{OC}) minus the voltage drop across the EEC model (where s is the Laplace operator), where I_{FC} is the fuel cell current:

$$V_{FC} = V_{OC} - R_s I_{FC} - \frac{R_1}{R_1 C_1 s + 1} I_{FC} \tag{2}$$

The model given in equation 2 is not linear due to the V_{OC} term. Equation 2 is therefore linearized, and the terms are collected as one fraction. The linear input / output dynamics for V_{FC} can thereby be described as the transfer function, where I_{CPI} is the pulse current:

$$\frac{V_{FC}}{I_{CPI}} = \frac{R_s R_1 C_1 \cdot s + (R_s + R_1)}{R_1 C_1 \cdot s + 1} \tag{3}$$

The transfer function given in equation 3, must be converted to the discrete time domain in order to apply the parameter estimation method to the model, where lower-case z is the z-domain operator and T_s is period of time between the samples. The discretization of the transfer function is necessary, since the parameter estimation method is to be implemented on a micro controller. The transfer function in equation 3, will be mapped into the discrete domain using the bilinear transform (Tustin):

$$s \leftarrow \frac{2}{T_s} \frac{z-1}{z+1} \tag{4}$$

The transfer function given in equation 3, is converted to the discrete time domain using equation 4:

$$\frac{V_{FC}}{I_{CPI}} = \frac{b_1 \cdot z^{-1} + b_2}{a_1 \cdot z^{-1} + 1} \tag{5}$$

where:

$$b_1 = \frac{T_s(R_1 + R_s) - 2R_S R_1 C_1}{2R_1 C_1 + T_s} \tag{6}$$

$$b_2 = \frac{2R_s R_1 C_1 + T_s(R_1 + R_s)}{2R_1 C_1 + T_s} \tag{7}$$

$$a_1 = \frac{T_s - 2R_1 C_1}{2R_1 C_1 + T_s} \tag{8}$$

The input / output dynamics for equation 5 can be described as a difference equation, where k indicates the k^{th} sample ($k \in \{1, 2, ..., N\}$):

$$V_{FC,k} = -a_1 V_{FC,(k-1)} + b_1 I_{FC,(k-1)} + b_2 I_{FC,k} \tag{9}$$

Based on the above an unknown parameter vector ($\hat{\theta}$) can be defined:

$$\underline{\hat{\theta}} = \begin{bmatrix} a_1 \\ b_1 \\ b_2 \end{bmatrix} \tag{10}$$

and a data row vector:

$$\underline{\phi}_k = \left[-V_{FC,(k-1)} \quad I_{FC,(k-1)} \quad I_{FC,k}\right] \tag{11}$$

The difference equation (9) can then be expressed as:

$$V_{FC,k} = \underline{\phi}_k \, \underline{\hat{\theta}} \tag{12}$$

The entire fuel cell voltage model output ($\underline{V}_{FC}$) with length N, can be described by replacing the data row vector with the entire dataset matrix $\left(\underline{\underline{\phi}}\right)$ in equation 12, where $\underline{\underline{\phi}}$ has the dimension of $N \times 3$).

In order to formulated the residual prediction error, described in equation 1, the formulation from above can now be inserted:

$$\underline{\epsilon} = \underline{V}_{FC} - \underline{\underline{\phi}} \, \underline{\hat{\theta}} \tag{13}$$

The residual prediction error vector given in 13 can now be squared, and minimized as a convex optimization problem, where the cost function ($J(\hat{\theta})$) is given as:

$$J(\hat{\theta}) = \underline{\epsilon}^T \underline{\epsilon} \tag{14}$$

$$= \left(\underline{V}_{FC}{}^T - \underline{\underline{\phi}}^T \, \underline{\hat{\theta}}^T\right)\left(\underline{V}_{FC} - \underline{\underline{\phi}} \, \underline{\hat{\theta}}\right) \tag{15}$$

It can be shown that the solution to the convex optimization problem given in eq. 15 is given by [23]:

$$\underline{\hat{\theta}} = \left(\underline{\underline{\phi}}^T \underline{\underline{\phi}}\right)^{-1} \underline{V}_{FC} \tag{16}$$

The estimated parameter vector ($\underline{\hat{\theta}}$) can now be converted back to the continuous EEC model parameters, by solving equations 6-8 for the parameters R_1, C_1 and R_s:

$$R_1 = \frac{2a_1b_2 - 2b_1}{a_1^2 - 1} \tag{17}$$

$$C_1 = \frac{T_s a_1^2 - 2T_s a_1 + T_s}{4b_1 - 4a_1 b_2} \tag{18}$$

$$R_s = \frac{b_1 - b_2}{a_1 - 1} \tag{19}$$

2.2. Experimental

To verify the CPI method, experiments have been conducted on a 10 cell SerEnergy high temperature PEM fuel cell short stack. The method can also be used for other sizes of fuel cells stacks, however this stack was available at the start of the experiment. For an increasing number of cells, the signal to noise ratio will be improved, but the method should be applicable from single cell to full stack. The stack was operated in a GreenLight Innovation test stand, with an external cooling cart for oil circulation. The stack consisted of 10 cells based on SerEnergy MEAs with an active area of 165 cm^2 and standard flow plates form a S165L SerEnergy stack.

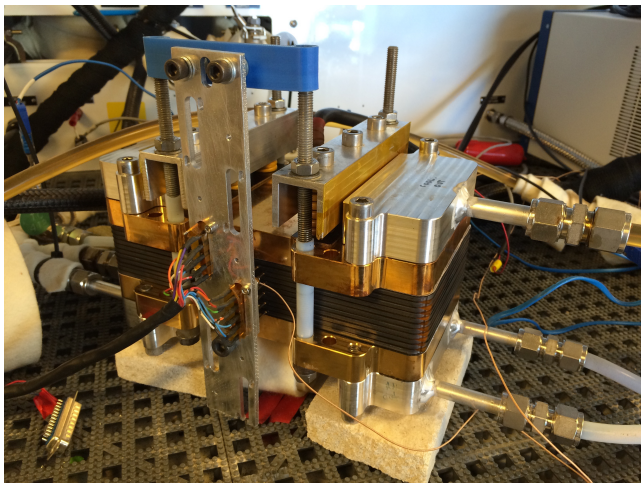

Figure 5: The 10 cell HT-PEM fuel cell stack, used for the experimental work.

The short stack is shown in Figure 5. It is heated and cooled by an external oil circuit at a forward temperature set point of 169 °C. The anode gas consists of dry hydrogen with a stoichiometric of λ_{H2}= 2, and the cathode gas consists of non-humidified atmospheric air from an air compressor, where the volume flow is controlled at stoichiometric ratio of λ_{air}=4. During the current pulses, the H_2 and air flows are not changed. This is done due to the fact that the bandwidth of the mass flow controllers are too slow compared to the frequency of the current pulses. Furthermore, the anode and cathode stoichiometric ratios are high enough to accommodate the extra current load. The anode and cathode gases are not preheated or pre-humidified.

The current is drawn from an external TDi RBL-488 electronic load with a 20 kHz bandwidth, which is controlled by a NI cRIO-9033 with a NI-9263 voltage output module. The internal data logging system in the GreenLight Innovation test stand is too slow for the purpose of this work, and therefore, cRIO is also utilized for data logging of the current and voltage. For voltage input a NI-9223 module was used for simultaneous measurements, with a sampling frequency of V_{FC} and I_{FC} of f_s=100 kHz. The sampling frequency is chosen high to make sure all dynamics are captured, and could be chosen lower for real life applications, however, this would require further investigation.

In order to compare the CPI method to the full impedance spectrum, EIS measurements were conducted in a galvanostatic mode using a Gamry reference 3000 potentiostat. The EIS measurements are performed at a starting frequency of 10 kHz and a final frequency of 0.1 Hz, with 10 points per decade. The AC perturbation current was fixed to 7.5 % of the DC value of the load current. The complex impedance function is given in equation 20:

$$Z = \frac{V_0 e^{j(\omega t - \varphi)}}{I_0 e^{-j\varphi}} = \frac{V_0 e^{-j\varphi}}{I_0} = Z_0(\cos\varphi - j\sin\varphi) \tag{20}$$

The impedance spectra are often interpreted by quantifying macroscopic fuel cell parameters using EEC model fits. Therefore, it is important to understand the general behavior of the analyzed fuel cell for the EEC model selection. In this work since the same model had to be used for fair comparison between the CPI method and the EIS method a simple EEC model as shown in Figure 4 was chosen. The impedance of and ideal resistor and capacitor can be calculated as follows:

$$Z_R = R \tag{21}$$

$$Z_C = \frac{1}{C(j\omega)} \tag{22}$$

3. Results and discussion

The CPI characterization method is demonstrated below based on the experimental data, and EEC model parameters were fitted using the method described in section 2.1.1.

3.1. Experimental data

During the test of the CPI method, the fuel cell stack was tested at the following DC levels:

$$i_{FC} = \{0.2, 0.3, 0.4\} \quad \text{Acm}^{-2}$$

which correspond to 32 A, 48 A and 64 A, respectively, for this size of fuel cell stack.

For testing the CPI characterization method, different amplitudes are tested to identify the effect of different current pulse amplitudes on the transient behavior. The amplitudes of the injected current pulses are:

$$I_{CPI} = \{1, 2, 3, 4, 5\} \quad \text{A}$$

As an initial experiment the CPI method was tested at different pulse frequencies. Figure 6 shows the data from an initial experiment, where the CPI method was tested at the following frequencies:

$$f_{CPI} = \{100, 10, 1, 0.1\} \quad \text{Hz}$$

It can be seen that at 100 and 10 Hz, the transient over potential is not fully developed. These frequencies are therefore not suited for this method, since the parameter estimation method descried in section 2.1 of this paper yields the best and most accurate performance if the transient voltage is fully developed. The time series data shown in Figure 6 are conducted with current pulses of 1 A, and the transient voltage behavior at different frequencies is representative for the remaining current pulse amplitudes.

For the frequencies 1 and 0.1 Hz, it can be seen that the transient voltage response is fully developed, as can be illustrated from the example of two pulses at 1 Hz with a duty cycle of 0.5 shown in Figure 7. These two frequencies can therefore be used for the parameter estimation of the electrical equivalent circuit. It can also be seen that in Figure 7 that the frequency could not e.g. be 2 Hz, since the period of steady state voltage level after the transient period would be cut off. It can also be seen in Figure 7 that the time the voltage is steady state is as long as the transient period during the pulses.

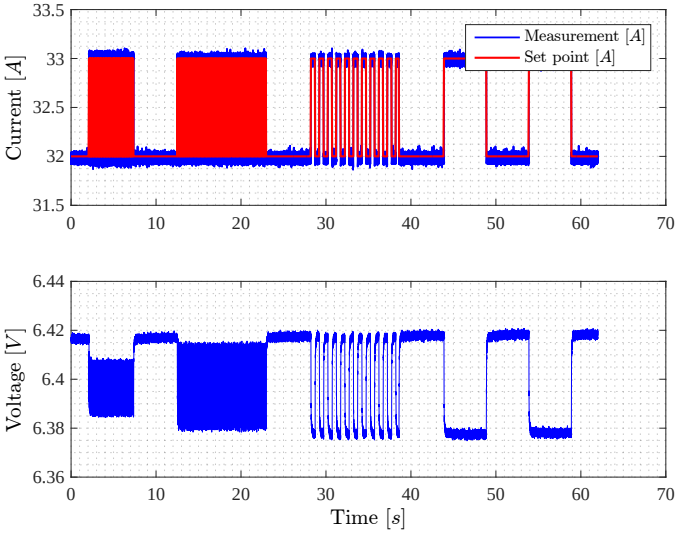

Figure 6: Time series of small current steps for the 1 A amplitude experiment, at different frequencies ($f_{CPI} = \{100, 10, 1, 0.1\}$ Hz).

When inspecting the 0.1 Hz data in Figure 6, it can be seen that the transient voltage is fully developed to a steady state level. At this frequency, the voltage is at steady state for the majority of the pulse time. This data could also be used for the parameter estimation, but the time required for one characterization experiment is 10 times longer than the 1 Hz data set. This is not a problem, when temperatures and operational parameters are constant during the characterization experiment, but by choosing the 1 Hz current pulses this uncertainty is eliminated. The 1 Hz current pulses seems to be a good trade-off, and are chosen for the parameter estimation.

3.2. CPI EEC model parameter estimation at different current pulse amplitudes

The CPI characterization method was tested based on the experimental data, at the two different DC current loads and at five different current pulse amplitudes.

In Figure 8 a typical dataset of two 1 A pulses, at a DC current density of 0.2 Acm^{-2} can be seen. The red dots are measured voltage data, and the blue line is the EEC model fit, where the EEC model parameters are estimated using the parameter estimation method described in section 2.1.1. The voltage response has been superpositioned by subtracting the DC value of the fuel cell voltage and by projecting the voltage signal into the positive plane. This is done in order to have a linear response, as described in section 2.1.1 and shown in Figure 8.

The time series window, where the parameters estimation was conducted is 2.1 s. It was kept constant for all the CPI tests to ensure comparability between them, meaning that two pulses at 1 Hz and a duty cycle of 0.5 are used for all CPI tests. The EEC model parameter estimation could also be done with different number of pulses, however two pulses were chosen as

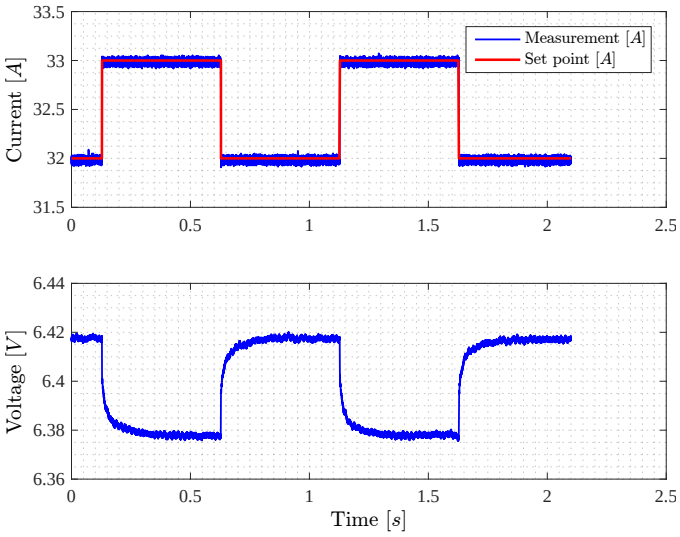

Figure 7: Selected time series data of two current pulses at 1 Hz (duty cycle=0.5), with 1 A current amplitude.

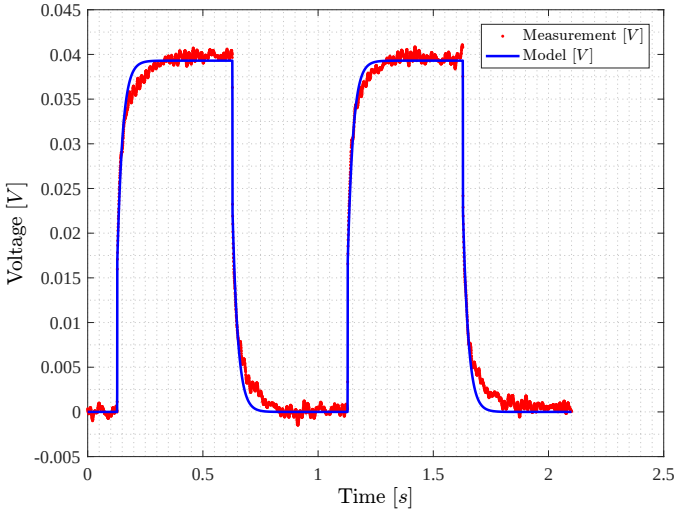

Figure 8: Selected time series data of 1 Hz (duty cycle=0.5) pulses, including the simple R-RC EEC model, at a 1 A current pulse amplitude.

a trade-off between sufficient data and low enough time span of the experiment.

In Figure 8, it can be seen that some noise is present. However, this noise is Gaussian, and can be considered as normal measurement noise, with a low amplitude of approximately 2 mV. The noise could be filtered, but this would change the amplitude of the abrupt voltage jump caused by the fuel cell stack series resistance. Furthermore, the signal to noise ratio is sufficiently low for the EEC model parameter estimation.

The blue model fit shown in Figure 8 is representative of the abrupt change of 17.5 mV, in the fuel cell stack voltage caused by the fuel cell stack series resistance. Hereafter, the voltage rise to 40 mV during a transient period. The first half of the transient voltage period shows a good fit to the model, but the second half of the transient period is slightly off. However, this EEC model fit is, as stated in section 2.1.1, the optimal solution to the parameter estimation problem. A more complex EEC model could yield a better model fit for the second half of the transient period, but this would require more fitting time and the authors found the solution to the parameter estimation problem of more complex EEC models to be unstable in some cases. Moreover, the sum of the resistances of the EEC model would be constant, independent of the EEC model structure.

In Tables 1, 2 and 3 are shown the results of the EEC model parameter estimation of the CPI characterization experiments at 0.2 Acm^{-2}, 0.3 Acm^{-2} and 0.4 Acm^{-2}, respectively.

Throughout all the three DC current loads, all the EEC model parameters are consistent with low parameter variance (σ^2). The variance of the parameters can be seen in the right column of the Tables 1, 2 and 3. The parameter variance is especially important when the measurement method is being used for fault detection, since a low variance can withhold a more aggressive threshold between faulty and non-faulty operation with relatively low probability of false alarm. The parameter variance is calculated as:

$$\sigma^2 = \frac{1}{N-1}\sum_{i=1}^{N}(\theta_i - \bar{\theta})^2 \tag{23}$$

where θ_i is the parameter R_s, R_1 or C_1, N is 5 since the variance is calculated for five different current pulse amplitudes and $\bar{\theta}$ is the arithmetic mean value of the parameter at different current pulse amplitudes.

In tables 1, 2 and 3, it can be seen that R_1 decreases with increase in current density. This is a common occurrence also in EIS measurements, where the spectrum spreads out with a decrease in DC current [24, 25]. This is in good agreement with the literature, and a proof that the suggested method can give similar results as can be obtained using the EIS method.

The value of the EEC model parameters are independent of the current pulse amplitude, between 1 – 5 A, which is the range of testing in this work. This is an advantage when the characterization method is physically implemented as suggested in Figure 3. The amplitude of the pulse will depend on the fuel cell voltage, which changes according to the polarization curve, which at its time changes with degradation. The amplitude of the current pulse will therefore be smaller at higher fuel cell stack load currents compared to the current pulse amplitude at lower load. It is important that the size of the resistor R_{CPI} is chosen small enough to accommodate sufficient signal to noise ratio. However, smaller current pulse amplitude also means a larger energy usage and the size of the current pulse should be limited in such a way that the anode and cathode stoichiometric ratios do not change, since these will affect the transient behavior of the fuel cell voltage, and thereby change the EEC model parameters. A constant flow of the anode and cathode gasses, will also ease the implementation of the method.

3.3. Comparison between CPI and EIS EEC model parameters

To validate the EEC model parameters identified using the CPI fuel cell characterization method, EIS measurements are

Table 1: Estimated EEC parameters for using the current pulse injection method at 0.2 Acm^{-2} DC fuel cell output current for 5 current pulse amplitudes.

	1 A	**2** A	**3** A	**4** A	**5** A	σ^2
$\mathbf{R}_s$ $[m\Omega]$	16.5	16.6	16.6	16.0	16.3	0.06
$\mathbf{R}_1$ $[m\Omega]$	22.8	22.6	22.5	22.9	22.4	0.04
$\mathbf{C}_1$ $[F]$	1.05	1.06	1.1	1.01	1.06	0.001

Table 2: Estimated EEC parameters for using the current pulse injection method at 0.3 Acm^{-2} DC fuel cell output current for 5 current pulse amplitudes.

	1 A	**2** A	**3** A	**4** A	**5** A	σ^2
$\mathbf{R}_s$ $[m\Omega]$	15.4	15.2	15.7	15.4	15.8	0.06
$\mathbf{R}_1$ $[m\Omega]$	17.9	17.6	17.4	17.4	17.5	0.04
$\mathbf{C}_1$ $[F]$	1.08	1.11	1.13	1.12	1.13	0.0004

Table 3: Estimated EEC parameters for using the current pulse injection method at 0.4 Acm^{-2} DC fuel cell output current for 5 current pulse amplitudes.

	1 A	**2** A	**3** A	**4** A	**5** A	σ^2
$\mathbf{R}_s$ $[m\Omega]$	15.2	15.0	15.1	15.1	14.9	0.01
$\mathbf{R}_1$ $[m\Omega]$	15.6	16.3	15.6	15.7	15.8	0.08
$\mathbf{C}_1$ $[F]$	1.16	1.21	1.17	1.19	1.15	0.0006

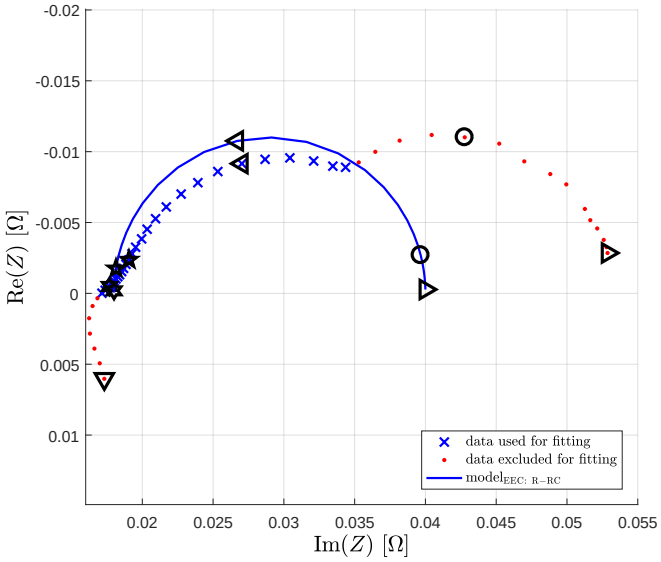

Figure 9: Simple R-RC EEC model fitted to high and intermediate frequencies. EIS data collected at 0.2 Acm^{-2} load current density. The black markers indicate the frequency decades $\{10k, 1k, 100, 10, 1, 0.1\}$ Hz.

conducted at each current load set point.

As it is known the low frequency part of the impedance spectra is related to the mass transport and the gas channel geometry [25]. The low frequency part of the measured impedance spectrum is therefore not represented in the impedance spectrum reassembled by the CPI EEC model parameters [26, 27, 28, 29]. When fitting EEC model parameters to the EIS data set, only the high and intermediate frequency points were considered. The experimental fuel cell EIS data in Figure 9 shows a clear boundary between the intermediate and low frequency data points in the range between the 10 and 1 Hz frequency markers, at around 2 Hz. Therefore, the fitting of the EIS EEC model parameters includes only data points above 2 Hz.

The fitting algorithm used for fitting the EIS EEC model parameters is a home made algorithm that utilizes a least square objective function and a Differential evolution optimization algorithm. The EIS fitted EEC model has been plotted using the entire frequency span (from 10k – 0.1 Hz) in order to show the low frequency intersection with the real axis on the Nyquist plot, as can be seen in Figure 9.

In Figure 9 an example of a model fit of the EIS data set can be seen. A more accurate model fit could have been accomplished using a constant phase element instead of the capacitor in the RC loop. However, since the EIS fitted EEC model parameters are to be compared to the CPI EEC model parameters, a capacitor has been used. The EEC model fitted to the EIS data, is the same model as used for the CPI method, and as illustrated on figure 4.

Since the same EEC model is fitted to both methods for comparison, the percentage deviations of the CPI EEC parameters from those of EIS EEC parameters is given in tables 4, 5 and 6, to show the validity of the CPI method compared to an established method, as EIS. At 0.2 and 0.3 Acm^{-2} the difference between the CPI and the EIS fitted EEC model resistances are low, with 2.3 % difference for R_s at 0.2 Acm^{-2} compared to the EIS fitted R_s parameter. The differences between the two are more pronounced at 0.4 Acm^{-2}, as can be seen in Table 6. However, they are within the same order of magnitude, and it can be concluded that the CPI characterization method can reproduce the EIS measurements for high and intermediate frequencies.

The EEC model parameters R_s and R_1 can be used as features for fault detection. Examples of faults signatures that can be based on the series resistance (R_s) and the polarization resistance (R_1), can e.g. CO contamination of the anode gas where an increase of polarization resistance can be observed [25, 30, 31, 32], for both low and high temperature PEM fuel cells. For both flooding and drying an increase in both the series resistance, polarization resistance and the mass transport resistance is reported to increase in the literature [33, 6, 34, 35]. The CPI impedance characterization method can therefore be used for detecting water management issues. However, since the CPI method do not capture the mass transport phenomena, the method might not be suited for early detecting, or an increased probability if missed fault.

4. Conclusion

In this work an EIS alternative to fuel cell characterization method has been investigated, namely the current pulse injection (CPI) characterization method. The proposed technique is a parameter estimation method for the electrical equivalent circuit (EEC) model parameters, based on the transient voltage response during current pulses, and can be said suitable for online use.

The method yields consistent EEC model parameter sets at different current pulse amplitudes, with low variance. The low variance makes the method attractive in fault detection systems, as it can minimize the probability of false alarm.

Table 4: Comparing the estimated EEC parameters using the CPI method and the EIS method at 0.2 Acm^{-2} DC fuel cell output current.

	1 A CPI	**EIS**	
$\mathbf{R}_s$	16.5 $m\Omega$	16.9 $m\Omega$	2.3 %
$\mathbf{R}_1$	22.8 $m\Omega$	23.6 $m\Omega$	3.4 %
$\mathbf{C}_1$	1.05 F	0.99 F	6 %

Table 5: Comparing the estimated EEC parameters using the CPI method and the EIS method at 0.3 Acm^{-2} DC fuel cell output current.

	1 A CPI	**EIS**	
$\mathbf{R}_s$	15.4 $m\Omega$	16.5 $m\Omega$	6.6 %
$\mathbf{R}_1$	17.9 $m\Omega$	18.2 $m\Omega$	1.6 %
$\mathbf{C}_1$	1.08 F	0.89 F	19 %

Table 6: Comparing the estimated EEC parameters using the CPI method and the EIS method at 0.4 Acm^{-2} DC fuel cell output current.

	1 A CPI	**EIS**	
$\mathbf{R}_s$	15.2 $m\Omega$	16.7 $m\Omega$	9 %
$\mathbf{R}_1$	15.6 $m\Omega$	16.9 $m\Omega$	7.7 %
$\mathbf{C}_1$	1.16 F	1.03 F	12.6 %

It can be concluded that the CPI fitted EEC model parameters can predict the impedance measurements similarly to the EIS fitted EEC model parameters, for the high and intermediate frequencies impedance loops. The EEC model estimated using CPI is generally simpler than what can be observed by EIS measurements, but could be sufficient for many diagnostics systems, such as the detection of drying or flooding of a low temperature PEM fuel cell stack, or it could be used for poisoning detection of CO contamination in the anode gas of a high temperature PEM fuel cell stack. However, it must be noted that the dynamic behavior of a low temperature PEM fuel cell is significantly faster, and the sampling frequency must therefore be chosen accordingly.

The characterization method can be implemented physically using a single resistor and transistor. This makes the solution attractive for mass deployment in fuel cell system diagnosis.

5. Acknowledgment

This work was funded by Innovation Fund Denmark in the framework of the 4M Centre.

References

[1] M. Becherif, H. S. Ramadan, K. Cabaret, F. Picard, N. Simoncini, O. Bethoux, Energy Procedia 74 (2015) 371–380. URL: http://dx.doi.org/10.1016/j.egypro.2015.07.629. doi:10.1016/j.egypro.2015.07.629.

[2] The Department of Energy, USA, Fuel cell technologies office multi-year research, Technical Report, 1, 2012. http://www1.eere.energy.gov/hydrogenandfuelcells/mypp/.

[3] P. Pei, H. Chen, Applied Energy 125 (2014) 60–75. doi:10.1016/j.apenergy.2014.03.048.

[4] R. Petrone, Z. Zheng, D. Hissel, M. C. Péra, C. Pianese, M. Sorrentino, M. Becherif, N. Yousfi-Steiner, International Journal of Hydrogen Energy 38 (2013) 7077–7091. doi:10.1016/j.ijhydene.2013.03.106.

[5] C. Jeppesen, M. Blanke, F. Zhou, S. J. Andreasen, in: IFAC-PapersOnLine, volume 48, Elsevier Ltd., 2015, pp. 547–553. doi:10.1016/j.ifacol.2015.09.583.

[6] N. Fouquet, C. Doulet, C. Nouillant, G. Dauphin-Tanguy, B. Ould-Bouamama, Journal of Power Sources 159 (2006) 905–913. doi:10.1016/j.jpowsour.2005.11.035.

[7] Z. Zheng, M. C. Péra, D. Hissel, M. Becherif, K. S. Agbli, Y. Li, Journal of Power Sources 271 (2014) 570–581. doi:10.1016/j.jpowsour.2014.07.157.

[8] M. A. Rubio, A. Urquia, S. Dormido, Journal of Power Sources 171 (2007) 670–677. doi:10.1016/j.jpowsour.2007.06.072.

[9] T. Mennola, M. Mikkola, M. Noponen, T. Hottinen, P. Lund, Journal of Power Sources 112 (2002) 261–272. doi:10.1016/S0378-7753(02)00391-9.

[10] G. H. Boyle, F. Goebel (1995).

[11] Y. Zou, X. Hu, H. Ma, S. E. Li, Journal of Power Sources 273 (2015) 793–803. doi:10.1016/j.jpowsour.2014.09.146.

[12] K. Propp, M. Marinescu, D. J. Auger, L. O'Neill, A. Fotouhi, V. Knap, G. J. Offer, G. Minton, S. Longo, M. Wild, V. Knap, Journal of Power Sources 328 (2016) 289–299. doi:10.1016/j.jpowsour.2016.07.090.

[13] C. E. Holland, J. W. Weidner, R. A. Dougal, R. E. White, Journal of Power Sources 109 (2002) 32–37. doi:10.1016/S0378-7753(02)00044-7.

[14] K. P. Adzakpa, K. Agbossou, Y. Dubé, M. Dostie, M. Fournier, A. Poulin, Ieee Transactions on Energy Conversion 23 (2008) 581–591. doi:10.1109/TEC.2007.914170.

[15] J. Cho, H. S. Kim, K. Min, Journal of Power Sources 185 (2008) 118–128. doi:10.1016/j.jpowsour.2008.06.073.

[16] F. Marignetti, M. Minutillo, A. Perna, E. Jannelli, IEEE Transactions on Industrial Electronics 58 (2011) 2420–2426. doi:10.1109/TIE.2010.2069073.

[17] S. Didierjean, O. Lottin, G. Maranzana, T. Geneston, Electrochimica Acta 53 (2008) 7313–7320. doi:10.1016/j.electacta.2008.03.079.

[18] H. Yu, C. Ziegler, Journal of The Electrochemical Society 153 (2006) A570–A575. doi:10.1149/1.2162450.

[19] P. T. Ha, H. Moon, B. H. Kim, H. Y. Ng, I. S. Chang, Biosensors and Bioelectronics 25 (2010) 1629–1634. doi:10.1016/j.bios.2009.11.023.

[20] C. de Beer, P. S. Barendse, P. Pillay, B. Bullecks, R. Rengaswamy, IEEE Transactions on Industrial Electronics PP (2014) 1–1. doi:10.1109/TIE.2014.2377131.

[21] J. R. Vang, S. J. Andreasen, S. S. Araya, S. K. Kær, International Journal of Hydrogen Energy 39 (2014) 14959–14968. doi:10.1016/j.ijhydene.2014.07.017.

[22] L. Ljung, System Identification: Theory for the User, 2nd ed., Prentice Hall, 1999.

[23] S. Shanmugan, A. M. Breipohl, Random Signals - Detection, Estimation and Data Analysis, Wiley Sons, Inc., 1988.

[24] J. L. Jespersen, E. Schaltz, S. K. Kær, Journal of Power Sources 191 (2009) 289–296. doi:10.1016/j.jpowsour.2009.02.025.

[25] S. J. Andreasen, J. R. Vang, S. K. Kær, International Journal of Hydrogen Energy 36 (2011) 9815–9830. doi:10.1016/j.ijhydene.2011.04.076.

[26] M. Chandesris, C. Robin, M. Gerard, Y. Bultel, Electrochimica Acta 180 (2015) 581–590. doi:10.1016/j.electacta.2015.08.089.

[27] I. a. Schneider, S. a. Freunberger, D. Kramer, A. Wokaun, G. G. Scherer, Journal of The Electrochemical Society 154 (2007) B383–B388. doi:10.1149/1.2435706.

[28] I. a. Schneider, S. a. Freunberger, D. Kramer, A. Wokaun, G. G. Scherer, Journal of The Electrochemical Society 154 (2007) B770. doi:10.1149/1.2435706.

[29] B.-T. Tsai, C.-J. Tseng, Z.-S. Liu, C.-H. Wang, C.-I. Lee, C.-C. Yang, S.-K. Lo, International Journal of Hydrogen Energy 37 (2012) 13060–13066. doi:10.1016/j.ijhydene.2012.05.008.

[30] F. Zhou, S. J. Andreasen, S. K. Kær, J. O. Park, International Journal of Hydrogen Energy 40 (2015) 14932–14941. doi:10.1016/j.ijhydene.2015.09.056.

[31] G. Nguyen, S. Sahlin, S. J. Andreasen, B. Shaffer, J. Brouwer, International Journal of Hydrogen Energy 41 (2016) 4729–4739. doi:10.1016/j.ijhydene.2016.01.045.

[32] T. Kadyk, R. Hanke-Rauschenbach, K. Sundmacher, Journal of Electroanalytical Chemistry 630 (2009) 19–27. doi:10.1016/j.jelechem.2009.02.001.

[33] D. Hissel, M. Pera, Annual Reviews in Control 42 (2016) 201–211.

500 doi:10.1016/j.arcontrol.2016.09.005.
[34] C. Cadet, S. Jemeï, F. Druart, D. Hissel, International Journal of Hydrogen Energy 39 (2014) 10613–10626. doi:http://dx.doi.org/10.1016/j.ijhydene.2014.04.163.
[35] A. Gebregergis, P. Pillay, R. Rengaswamy, IEEE Transactions on Industry
505 Applications 46 (2010) 295–303. doi:10.1109/TIA.2009.2036677.